Geophysical Journal International

Geophys. J. Int. (2014) **196,** 447–460
Advance Access publication 2013 November 10

doi: 10.1093/gji/ggt374

Seismic velocity changes, strain rate and non-volcanic tremors during the 2009–2010 slow slip event in Guerrero, Mexico

Diane Rivet,[1,*] Michel Campillo,[1] Mathilde Radiguet,[1] Dimitri Zigone,[1] Victor Cruz-Atienza,[2] Nikolai M. Shapiro,[3] Vladimir Kostoglodov,[2] Nathalie Cotte,[1] Glenn Cougoulat,[1] Andrea Walpersdorf[1] and Eric Daub[1]

[1] *ISTerre, Université Joseph Fourier, Maison des Géosciences, BP* 53, *F*-38041 *Grenoble, France. E-mail: rivet@ipgp.fr*
[2] *Instituto de Geofísica, Universidad Nacional Autónoma de México, CU, Coyoacan,* 04510 *México, D.F., México*
[3] *Institut de Physique du Globe de Paris, Sorbonne Paris Cité, CNRS (UMR*7154*),* 1 *rue Jussieu, F*-75238 *Paris, cedex* 5*, France*

Accepted 2013 September 16. Received 2013 September 10; in original form 2012 November 28

SUMMARY

We use ambient noise cross-correlations to monitor small but reliable changes in seismic velocities and to analyse non-volcanic tremor (NVT) intensities during the slow slip event (SSE) that occurred in 2009 and 2010 in Guerrero. We test the sensitivity of the seismic velocity to strain variations in absence of strong motions. The 2009–2010 SSE presents a complex slip sequence with two subevents occurring in two different portions of the fault. From a seismic array of 59 seismometers, installed in small antennas, we detect a velocity drop with maximum amplitude at the time of the first subevent. We analyse the velocity change at different period bands and observe that the velocity perturbation associated with the SSE maximizes for periods longer than 12 s. Then a linearized inversion of the velocity change measured at different period bands is applied in order to determine the depth of the portion of the crust affected by this perturbation. No velocity change in the first 10 km is detected. Below, the velocity perturbation increases with depth, affecting the middle and lower crust. Finally, we compute the transient deformation produced by the SSE in an elastic model using the slip evolution recovered from the inversion of continuous GPS. The comparison between the velocity changes and the deformation suggests that the velocity change is correlated with the strain rate rather than with the strain. This result is similar to what was observed during the 2006 SSE in the same region and suggests a non-linear behaviour of the crust.

The velocity changes can be interpreted together with other observables such as NVTs. During the 2009–2010 SSE we measure NVT activity using continuous seismic records filtered between 2 and 8 Hz. We observe a correlation between velocity changes (for period band greater than 14 s) and tremor activity whereas no correlation exists between velocity changes and seismic noise energy measured at long periods. These observations suggest that both seismic velocity change and NVT can be used as indication of transient deformation at depth.

Key words: Wave scattering and diffraction; Rheology and friction of fault zones; Subduction zone processes.

1 INTRODUCTION

Non-volcanic tremor (NVT) and slow slip events (SSE) are observed in many active plate boundaries around the world (e.g. review of Schwartz & Rokosky 2007). SSEs are transient aseismic slips that contribute to release the accumulated elastic strain at the plate interfaces. SSEs are usually accompanied by NVT episodes, which are weak seismic signals of long duration, persistent in time and coherent over many stations (Obara 2002; Rogers & Dragert 2003; Obara *et al.* 2004). The data acquired on these two geophysical processes reveal a wide diversity of behaviours that vary from one region to another. For instance, in Cascadia and Southwest Japan subduction zones a clear temporal and spatial correlation between NVT and SSE has been observed and called episodic tremors and slip (ETS;

*Now at: Institut de Physique du Globe de Paris, Sorbonne Paris Cité, CNRS (UMR7154), 1 rue Jussieu, 75238 Paris, cedex 5, France.

Rogers & Dragert 2003; Obara *et al.* 2004). In other subduction zones like Costa Rica (Brown *et al.* 2005), Alaska (Ohta *et al.* 2006; Peterson & Christensen 2009) and Mexico (Payero *et al.* 2008; Kostoglodov *et al.* 2010) the association of SSE and NVT does not seem systematic. Moreover, in areas like the Hikurangi subduction margin, New Zealand (McCaffrey *et al.* 2008; Delahaye *et al.* 2009) and the Boso Peninsula of Japan (Ozawa *et al.* 2007), even no NVT was observed during slow slip. However, the recent detection of NVT at the northern Hikurangi margin associated with the 2010 Gisborne SSE suggests that the thick accumulation of highly attenuating sediment in the accretionary wedge inhibits the NVT detection in some cases (Kim *et al.* 2011). According to the classification proposed by Obara (2011), SSEs in Mexico belong to long-term SSE considering their duration and their updip position in the trench as shown by Vergnolle *et al.* (2010) and Radiguet *et al.* (2011). Long-term SSEs are also observed in the Bungo Chanel in Southwest Japan and trigger neighbouring downdip NVT activity (Hirose *et al.* 2010). The authors suggest that long-term SSE could activate downdip short-term SSEs, which could remain undetected by GPS, and synchronized with NVT. Besides, some studies locate tremors at the plate interface as suggested in Japan (e.g. Shelly *et al.* 2006; Ohta & Ide 2008), while in other studies it was proposed that they are located within the overriding plate like in Cascadia (Kao *et al.* 2005), Japan (Nugraha & Mori 2006) and Mexico (Payero *et al.* 2008). However this discrepancy in the depth of NVTs in those subduction zones may arise from the locating methods. Different mechanical processes are invoked to explain tremor's generation, but an accurate NVT depth estimate is required to discriminate their possible physical models. The two predominant models of NVT, as described by Rubinstein *et al.* (2010) are: (1) frictional processes with shear rupture of some portion of a fault undergoing slow slip and (2) fluid processes, with fluid flow at the plate interface and within the overlying plate. For the later model deshydratation from basalt to eclogite of the subducting slab would increase the fluid pressure causing sequence of hydraulic fracturing recorded at the surface as long and emissive seismic signals (Obara 2002). Rogers & Dragert (2003) argue that the resonating walls of fluid conduits near the plate interface could also produce tremor like signals recorded at the surface.

In the Guerrero region, Mexico, several observations suggested a complex behaviour of NVT activity in relation with SSEs. The 2006 SSE that occurred in the region had a significant seismic moment magnitude ($M_w = 7.4$ for the 2006 event according to Radiguet *et al.* 2011; Larson *et al.* 2007). During this SSE, the activity of the NVT increased but the NVT area was separated spatially from the slipping portion of the interface (Kostoglodov *et al.* 2010). Besides, significant NVT episodes occurred during the inter-SSE period (Kostoglodov *et al.* 2010). Finally, Rivet *et al.* (2011) observed a transient velocity change during this SSE that was strongly correlated with the maximum of the dilation rate induced by the SSE, and that they interpreted as a non-linear elastic response of the crust.

In this work we investigate the relation between seismic velocity changes, and the NVT activity during the 2009–2010 SSE. We will focus particularly on the relation between changes of velocity, the deformation produced by the SSE, and the NVT activity. For this purpose, we propose to use seismic velocity changes as a proxy of the strain rate.

The 2009–2010 SSE started in 2009 July (Walpersdorf *et al.* 2011). The surface displacements observed from the GPS time-series are lower than those observed during the 2006 SSE (Walpersdorf *et al.* 2011). However the slip duration for this SSE is longer, about 14 months against 6 months for the previous event. It also presents a more complex slip sequence. From GPS observations, Walpersdorf *et al.* (2011) and Radiguet (2011) showed that the SSE broke in two steps, with two separate portions of faults that have dislocated successively. The first event broke a patch of the subduction interface located in the southwest part of the Guerrero state and the second one started at the end of 2010 February and took place in the southeast part of Guerrero (Fig. 1). Zigone *et al.* (2012) proposed that this second subevent was actually triggered by teleseismic surface waves generated by the giant M8.8 Maule (Chile) earthquake of 2010. The 2009–2010 SSE is thus interesting in the sense that it allows to assess the sensitivity of the detection of small crustal velocity perturbation during this complex SSE, which has a smaller slip rate than the 2006 SSE (40 cm yr^{-1} vs. $\sim$70 cm yr^{-1}).

These observations of velocity change during the SSE are important for two reasons: first, velocity changes are clearly related to the strain rate perturbation produced at depth by the SSE. Secondly, using velocity changes as a proxy of the strain rate, we can investigate the relation between NVT and the state of deformation of the overriding plate.

2 DATA AND METHOD

2.1 Seismological data

We use seismic records from a temporary network of nine seismic mini-arrays deployed since 2009 in the framework of the French–Mexican G-GAP project (Table 1) complemented with four broad-band stations of the Mexican National Seismological Service (SSN) network (Table 2). Four mini-arrays consist of a broad-band sensor (CMG40 of Guralp) in the centre, surrounded by six or three short period sensors with an aperture of approximately 150 m, for example, XALI mini-array (Fig. S1). The other five mini-arrays consist of groups of three to six short period sensors. Overall, we have 59 sensors (eight broad-band) located nearby the city of Iguala in the northern part of the Guerrero state (Fig. 1). Although we have a rather dense array, recording periods vary from one station to another and not always cover the entire duration of the SSE. We measure velocity changes for the period band between 4 and 27 s, however, most of the sensors we use in this study are short period sensors. At long period, the instrument responses of those sensors show an important bias in the phase and error in the amplitude of the signal. However, because these errors are constant over time, they do not affect the relative interstation phase shift we measure on the noise cross-correlations. Brenguier *et al.* (2008a,b) demonstrated the feasibility of using exclusively short period sensors to measure velocity changes on the San Andrea fault in the Parkfield area and on the Piton de la Fournaise volcano at La Reunion island. In this analysis we make reliable measure down to 27 s using mainly short period sensors.

The procedure for data processing and computing seismic noise correlations in different period bands is described thereafter. After high-pass filtering, we eliminate portion of signals with amplitude greater than 10 times the standard deviation calculated for the day. We then apply spectral whitening between 1 and 30 s on all daily noise records. We bandpass filter continuous signals in two period ranges: 4–16 and 8–30 s. To remove small earthquakes, signals with amplitude greater than three times the standard deviation are then discarded. Finally, we apply 1-bit temporal normalization on the two sets of noise signals filtered in the period band 4–16 and 8–30 s. By doing so we prevent bias due to the 1-bit normalization that can

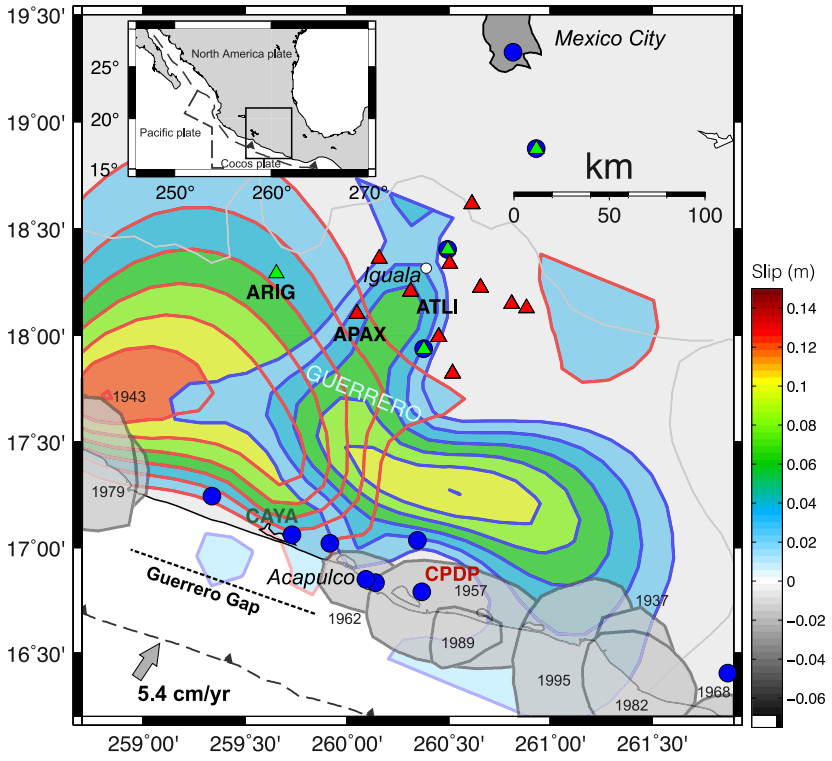

Figure 1. Inset: square is a study region, the Guerrero state, Mexico. Green triangles indicate the positions of broad-band seismic stations (SSN) used in our analysis. The red triangles show the positions of seismic mini array network consisting of a broad-band station surrounded by at least three short period sensors. The blue circles show the GPS stations. The shaded areas indicate the rupture areas of large earthquakes that occurred during the previous century. The dashed line represents the Middle America trench. The gray arrow shows the convergence rate between the Cocos and North America plates (DeMets *et al.* 1994). The colours represent the slip amplitude for the 2009–2010 SSE. Red and blue contours delimit the slip contours during the first subevent and the second subevent respectively (Radiguet 2011).

Table 1. List of the mini-arrays of the G-GAP seismic network.

Station name G-GAP array	Latitude (°N)	Longitude (°E)	Number of broad-band sensors	Number of short period sensors
AMAC	18.6066	−99.3843	1	6
APAX	18.0913	−99.9490	1	6
ATLI	18.1963	−99.6853	1	6
XALI	17.9830	−99.5471	1	6
ATEN	18.1175	−99.1156	0	3
CACA	18.2147	−99.3422	0	6
COAC	18.1373	−99.1889	0	6
HUIZ	17.8119	−99.4797	0	6
TELO	18.3500	−99.8393	0	3
TOMA	18.3271	−99.4933	0	3

Table 2. List of the broad-band stations of the Mexican Seismological National Service used in this study.

Station name SSN array	Latitude (°N)	Longitude (°E)
ARIG	18.2805	−100.3437
MEIG	17.9252	−99.6197
PLIG	18.3923	−99.5023
YAIG	18.8623	−99.0671

occur if applied on broad-band signals. Records are then correlated for all pairs of stations and for everyday. We obtain two sets of correlations in the two period bands 4–16 and 8–30 s. To measure seismic velocity variations, we bandpass filter the correlations in different period bands (Table 3). For all period bands lower than the 13–17.9 s band, we used correlations measured from the noise filtered in the 8–30 s period band. We often refer to the central period, which is the centre of the period band of the cross-correlations.

Table 3. List of period bands used to filter cross-correlations before measuring velocity changes.

Minimal period (s)	Maximal period (s)	Central period (s)
4.0	5.50	4.75
5.0	6.80	5.90
6.0	8.00	7.00
7.0	9.56	8.28
8.0	11.00	9.50
9.0	12.30	10.65
10.0	13.70	11.85
11.0	15.15	13.07
12.0	16.50	14.25
13.0	17.90	15.45
14.0	18.90	16.45
15.0	20.00	17.50
16.0	22.00	19.00
17.0	23.30	20.15
18.0	24.70	21.35
19.0	26.00	22.50
20.0	27.00	23.50

2.2 Measurements of velocity change

Seismic velocity changes in the Earth's crust indicate changes in the elastic properties related to the stress field variations in time. A

continuous monitoring of the seismic velocity within the crust thus provides a measure of the mechanical state of the crust. This continuous monitoring is achieved through the use of seismic noise, which illuminates continually the crust. The possibility to recover Green's functions from the cross-correlations of random seismic wavefields such as seismic coda (Campillo & Paul 2003) and seismic noise (Shapiro & Campillo 2004) has been recently demonstrated. From the monitoring of the reconstructed seismic waves traveltimes it is possible to recover the relative seismic velocity change in the area of interest. A robust feature of this seismic noise based technique is that reliable measures of velocity changes can be achieved even when the full reconstruction of the Green's function from the cross-correlation has not been reached yet (Hadziioannou *et al.* 2009; Weaver *et al.* 2009).

From continuous seismic noise records we compute correlations between all pairs of stations in the Guerrero region for consecutive periods of time. These correlations are calculated between vertical components over a 40-d window that is shifted every 10 d, from 2009 May to 2011 May. From the correlations computed from the vertical components of noise records, we retrieve mainly Rayleigh waves. Fig. S2 presents the 40-d cross-correlation functions computed between two broad-band stations and two short period sensors. The stability of the cross-correlations for the long period 8–30 s between short period sensors is compared to the one obtained from broad-band sensors. It can be observed that the bias in the phase introduced by the short sensors is constant and that later arrivals in the coda of the cross-correlations are stable over time.

The reference cross-correlation, for a given pair of stations is defined as the average of all correlations during the entire recording period. This reference can be interpreted as the average background state of the surrounding medium. Using the same approach as for repeating earthquakes (e.g. Poupinet *et al.* 1984), seismic velocity change is obtained from the comparison of the current cross-correlation function, computed for a given time, with the reference cross-correlation. Under the first-order assumption of a homogeneous perturbation in the crust, the relative difference in traveltime gives the relative change in the seismic velocity: $\mathrm{d}v/v = -\mathrm{d}t/t$.

For any couple of reference cross-correlation and current cross-correlation functions, the time delay between the two signals is measured on the coda waveforms from multiply scattered waves. It exists two different approaches to measure these delays. First, the Stretching method proposed by Lobkis & Weaver (2003) in laboratory ultrasonics, consists in stretching the whole coda of the current signal by a factor ε until the correlation coefficient between this signal and the coda of the reference reaches a maximum. For this particular value of the ε we retrieve the temporal dilation $\varepsilon = \mathrm{d}v/v$. The distortion between two waves form is given by the maxima of the correlation coefficient if less than 1.

Second, the Multiple window Spectral Analysis method originally proposed by Poupinet *et al.* 1984, also called Doublets method (e.g. Brenguier *el al.* 2008a,b) measures apparent delays $\mathrm{d}t(t)$ within a series of short time overlapping windows at several distinct time t. These $\mathrm{d}t(t)$ are determined from the phase shift measurements and a cross spectrum analysis in the frequency domain. The slope $\mathrm{d}t(t)$ of the distribution of $\mathrm{d}t(t)$ measures reveals a change in the medium $\mathrm{d}v/v = -\mathrm{d}t/t$. A measure of a coherency between two windowed signals on the coda allows to eliminate signals with insufficient signal-to-noise ratio. In addition, a least-squares error is estimated for each distribution of $\mathrm{d}t(t)$ for every cross-correlations. In this approach, the delay is independent of the fluctuations of the energy spectrum of the correlation. Finally, we average the relative velocity changes for all pairs of stations and repeat this computation for different period bands. In the doublet method, the reliability of the velocity change measurements is estimated from both the coherency measured between the reference and the 40-d stacked cross-correlation functions and the statistical error of the linear regressions $\mathrm{d}t(t)$ averaged for all the correlations (Clarke *et al.* 2011).

A major limitation of the seismic noise correlation method to monitor geological structures comes from the irregular distribution of noise sources and their variations over time. Noise sources in the microseismic period ranges are mainly concentrated in oceanic regions (Stehly *et al.* 2006; Tanimoto *et al.* 2006; Koper *et al.* 2009; Stutzmann *et al.* 2009; Landès *et al.* 2010; Schimmel *et al.* 2011; Hillers *et al.* 2012) and depend on seasons and climatic events such as storms. In Supporting Information (see Fig. S3), we propose a study of the normalized background seismic energy flow and its variations over time in the period band we use in the velocity changes analysis.

Weaver *et al.* (2009) and Froment *et al.* (2010) showed that the anisotropic distribution of noise could produce an error of 1 per cent in the measurement of traveltimes for the ballistic waves reconstructed from the noise cross-correlations. On the other hand, the change in traveltime induced by a change in velocity of the medium is less than 1 per cent (e.g. Wegler & Sens-Schonfelder 2007; Brenguier *et al.* 2008a,b; Chen *et al.* 2010; Rivet *et al.* 2011). It is therefore essential to overcome the bias introduced by seasonal variations of noise sources.

To reduce the errors caused by possible variations of the noise source positions, we measure the traveltime delays on coda waves of the correlations. The coda window is defined between 5 s after the arrival of the direct wave and 90 s. The coda is made up of diffuse waves scattered on the heterogeneities of the crust and thus tend to lose the source signature. Traveltime delay measured within the coda is less sensitive to source variations.

2.3 Selection of correlations based on their signal-to-noise ratio

We use the signal-to-noise ratio estimations to make an automatic selection of daily correlations. From the reference correlation computed between two stations, we measure the time of the maximum of the envelope signal. This gives us a good approximation of the position of the Rayleigh wave reconstructed for each daily correlation. We then calculate the ratio between the Rayleigh wave amplitude and the amplitude of the incoherent signal (noise) for each daily correlation. The Rayleigh wave average amplitude is calculated on a 20 s window centred on the maximum amplitude; the average amplitude of the incoherent signal is measured for long time lapse on a window of 50 s between 190 and 240 s of the correlation signal. Daily correlations with a signal-to-noise ratio greater than 1.5 are then averaged over periods of 40-d with an overlap of 10 d to obtain stable traces with higher signal-to-noise ratio. Fig. S4 presents daily cross-correlations for the AMAC3–APAX4 pair of stations before and after the selection based on the signal-to-noise ratio. By averaging the daily correlations over 40 d, the signal-to-noise ratio increases by a factor $\sqrt{40} \approx 6$. We thus expect the stacked signals to reach a signal-to-noise ratio greater than 10.

2.4 Reliability of the velocity change measurements

The seismic network used in this study consists of broad-band and short period stations belonging to two separate networks with

important variations over time of the number of stations available. We use both the Multiple Window Spectral Analyse method and the Stretching method described above to check the reliability of our velocity change measurements. Changes over time are estimated from all 40-d stacks of cross-correlations in the 8–20 s period band. The results obtained with both methods are in good agreement (Fig. S5). This confirms the robustness of the measured traveltime changes despite the large variations over time of the number of pairs of stations (Fig. 2c).

Weaver *et al.* (2011) established a theoretical expression to estimate the error of velocity change computed on noisy measurements. This expression is a function of the central frequency, the bandwidth, the length of the windowed coda and the coherency between the stretched correlation at a given time and the reference one. For correlations computed from consecutive period of 40 d of noise at 8–20 s period band, using the theoretical expression of Weaver *et al.* (2011) we find that the velocity change fluctuation due to the noisy component of the signals we use is 1.8×10^{-3} while the largest variation observed during SSE reaches 8×10^{-3}.

3 RESULTS

A long-term variation of seismic velocity is observed during the SSE (Fig. 2). This SSE does not emit any seismic waves susceptible to affect the surface layers of the crust and cause superficial velocity change. Similarly to the 2006 SSE (Rivet *et al.* 2011), the 2009–2010 SSE affects the medium at depth only through the slow deformation it produces. However the GPS time-series during this SSE show that the SSE had a complex slip sequence with two portions of the fault that slipped successively (Radiguet 2011; Walpersdorf *et al.* 2011). Fig. 2(a) presents the surface displacements during the SSE at the GPS stations CPDP and CAYA (GPS locations are shown in Fig. 1). The first subevent that occurred on

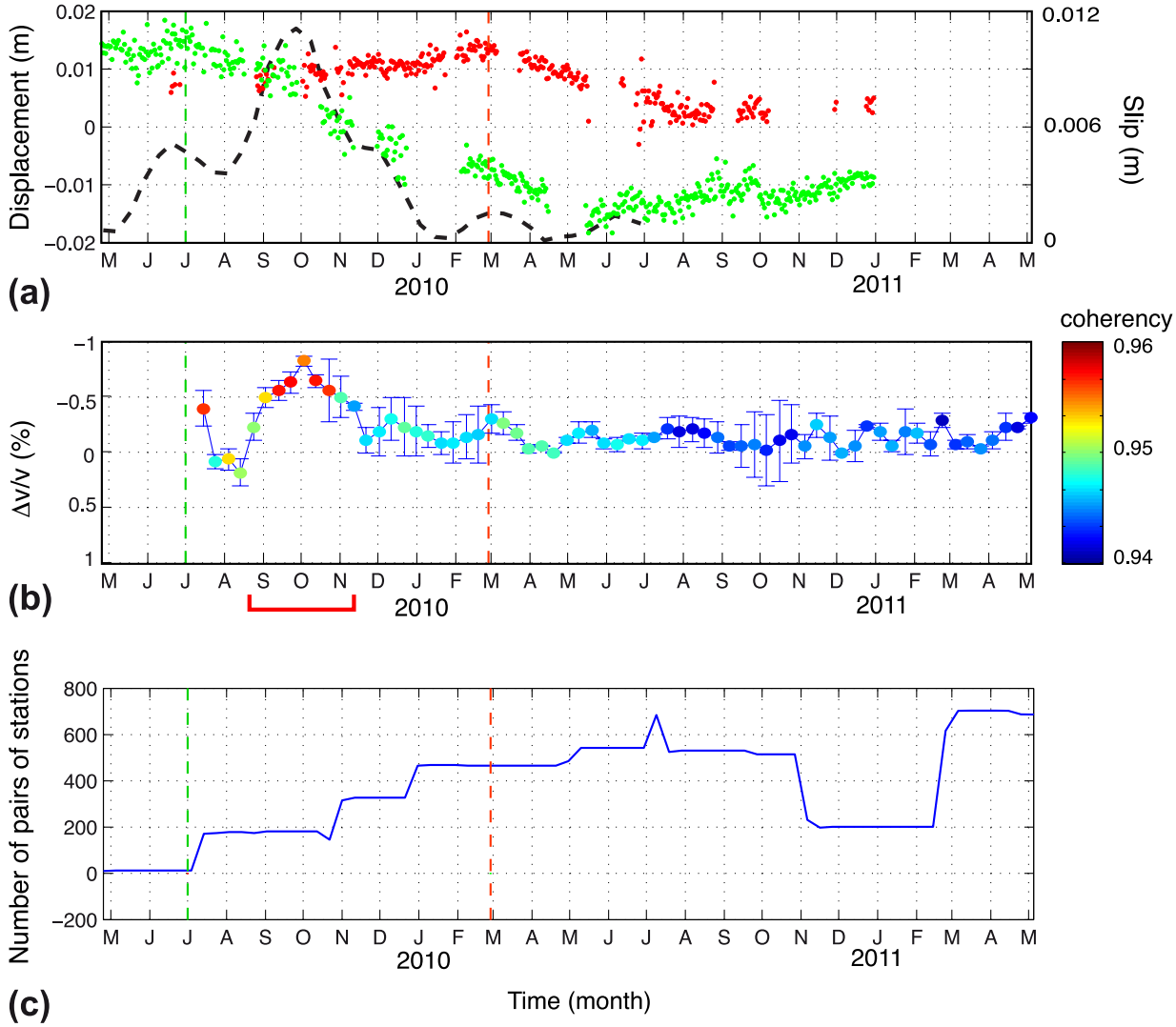

Figure 2. Comparison between the seismic velocity perturbation and the 2009–2010 SSE. (a) Time-series of daily north–south displacements recorded at CPDP (red) and CAYA (green) GPS stations with respect to ITRF2008 (Altamimi *et al.* 2011) and cumulated slip over 10 sequential days (dashed line) at the plate interface below APAX station (Radiguet 2011). (b) Seismic velocity change measured using the Doublets method from the vertical components of the correlations measured between pairs of stations at 15–20 s period band. The red bracket indicates the largest variation observed between 2009 September and November. Error bars represent the average least-squares error on the linear regressions of $d\tau(t)$ computed to measure the relative velocity change dv/v in the Doublet method. (c) Number of pairs of stations used to perform the velocity change measurement as a function of time. The red and green dashed lines represent respectively, the initiation of the first and second subevent of the SSE.

the western part of the Guerrero subduction interface produced a slip that started in mid-2009 and was detected on CAYA station, whereas the second subevent, that happened on the eastern part produced a slip that started in early 2010 March and was detected on stations located to the east, for example, CPDP. Fig. 2(b) shows the seismic velocity evolution estimated in the 15–20 s period band during the SSE. We observe a decrease of about 0.8 per cent of the seismic velocity between 2009 September and November during the first subevent. The seismic velocity changes observed here do not correlate with the number of available station pairs (Fig. 2c). Besides, to verify that the velocity change at long period is reliably measured using mainly short period sensors, we compare the velocity change from seven broad-band stations with the velocity change measured from 51 short period sensors (Fig. S6). Despite higher fluctuation of the velocity change measurements due to a limited number of correlations, the main perturbation between 2009 September and November is detected for each subset of stations.

Radiguet (2011) was able to model the evolution of the slip on the subduction interface during the SSE (Fig. S7) from the GPS time-series inversion using the Principal Component Analysis Inversion Method (PCAIM) developed by Kositsky & Avouac (2010). Through a comparison between the variations of seismic velocity (Fig. 2b) and the slip velocity of the SSE (Fig. S7), we observe that the major reduction in wave speed corresponds to the period of highest slip rate between 2009 September and November.

3.1 Seismic velocity changes at different frequency bands

To constrain the extension of the velocity perturbation at depth, we measure the seismic velocity changes using the records filtered in different period bands listed in Table 3, from 4–5.6 to 20–27 s (Fig. 3). It has been shown both theoretically and observationally that the seismic coda has average properties described by the equipartition of the propagation modes (Hennino *et al.* 2001; Margerin *et al.* 2009). As a result, the coda recorded at the surface is dominantly composed of surface waves. In the case of noise cross-correlations computed from the vertical component records, we recover mainly Rayleigh waves. The global sensitivity of coda wave to velocity changes at depth in a given time window depends on the proportion of the traveltime spent as each type of waves for all contributing paths. At the first order, we consider only the dominant surface waves and we expect that the traveltime delays measured on the coda of the cross-correlation functions depend on periods similarly to the surface waves: shorter periods are sensitive to shallower structures while longer periods sample deeper in the crust. This hypothesis is supported by numerical tests on the sensitivity of coda waves delayed by a velocity change at depth (Obermann *et al.* 2013). The authors investigated the sensitivity at depth of the coda waves to local velocity perturbation in a 2-D numerical wavefield simulation. They showed that the depth sensitivity of the coda waves is a combination of bulk-wave sensitivity and surface wave sensitivity. The partitioning ratio of bulk and surface wave sensitivities depends on the lapse time in the coda among other factors. Surface waves dominate the coda sensitivity for about six mean free times, while body waves dominate the later coda. The Earth's crust is a weakly scattering medium with long mean free times for long period seismic waves (e.g. >5 s)—in fact teleseismic records indicate that the long-period waves remain coherent for long traveltimes. Working at low frequency and at early times in the coda as it is done here implies that our observations of velocity changes can be interpreted using the sensitivity of surface wave. Therefore, the depth sensitivity of the velocity change measurements during the SSE can be approximated by surface waves sensitivity. Velocity variations obtained for periods around 14 s have a high sensitivity within the middle crust but this sensitivity decreases towards the subduction interface (∼40 km in Guerrero, Fig. S8). Therefore, variation in speed measured at around 14 s period indicates a significant change of the medium induced by deformation at mid-crustal depth.

During the 2009–2010 SSE for central periods smaller than 8 s, velocity fluctuations are smaller than the noise level (−0.1 per cent) implying that we detect no measurable seismic velocity variations (Fig. 3a). On the other hand, for wave speed variations calculated at periods between 8 and 18 s of central period, there was a rapid decrease of the seismic velocity in 2009 July. Although this variation has large amplitudes (−0.8 per cent), the perturbation disappeared after about 3 months. It is impossible to detect precisely the onset of this perturbation because no sufficient data were acquired before 2009 July. After the velocity rises close to its average value in August, a long and major seismic velocity decrease affects the medium between 2009 September and November. This perturbation that reaches −0.8 per cent is particularly visible between for all period bands between 12 and 24 s of central period. At longer period, beyond 24 s, it is possible that this decrease of velocity still exists. However, with our data set dominated by short period sensors, the measurement of the velocity perturbation becomes unstable at long periods. Besides, weak scattering at long period limits the signal-to-noise ratio in the coda because of the lack of late energetic arrivals, which would accumulate delays large enough for precise measurements.

We can distinguish another velocity change of smaller amplitude (−0.4 per cent) in 2010 March, observed between 12 and 24 s of central period. This change may reflect the slip initiation of the second subevent. Unlike for the main perturbation of the velocity, the slip model proposed by Radiguet (2011) does not have enough resolution to relate this last velocity variation to a clear episode of high slip rate. Fig. 3(b) represents the average least-squares error on the linear regressions of $\mathrm{d}t(t)$ computed to measure the relative velocity change measure $\mathrm{d}v/v$ in the Doublet method. At the time and within periods band of the dominant perturbation, that is, from 2009 September to November and between 12 and 24 s period, the error is stable and varies between 0.1 and 0.2 per cent (Fig. 3b). This confirms the reliability of the velocity changes observed between 2009 September and November and in 2010 March.

To ensure that the measured velocity variations are independent of the variations of the noise energy, we compute the correlation coefficients between the velocity variations and the noise energy measured at 10–20 s period band. The noise energy is estimated from the squared velocities of the vertical component for stations ARIG, ATLI and APAX and then is averaged over these stations. A median filter of 40-d time window was applied to the long period noise signal. Figs 4(a)–(c) shows the evolution of both the noise energy and the seismic velocity variations calculated for three different period ranges 5.0–6.8, 13–17.9 and 19–26 s with central period, respectively, of 5.9, 15.4 and 22.5 s. Fig. 4(d) summarizes the correlation coefficients for all velocity change measured for the 17 period bands listed in Table 3. The correlation coefficient is close to zero at periods longer than 12 s for which we observe a velocity change. The correlation between changes in the wave speed and noise energy is somewhat higher for shorter periods between 6 and 8 s for which we do not observe velocity change during the SSE. This analysis shows that the observed seismic

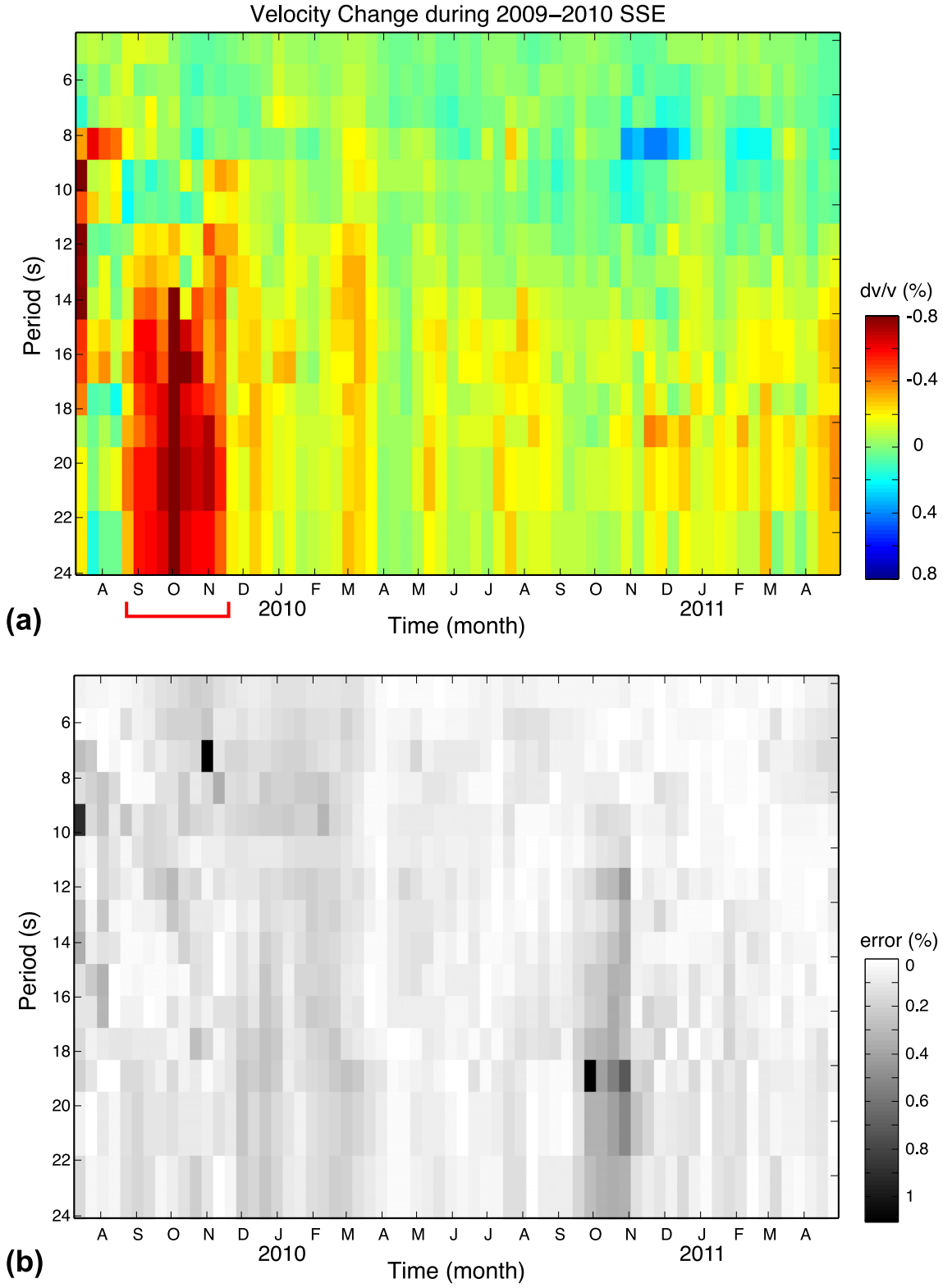

Figure 3. (a) Relative seismic velocity change ($d\upsilon/\upsilon$) as a function of the central period around which the correlations were filtered. The red bracket indicates the largest variation observed between 2009 September and November. (b) Average least-squares errors on the linear regressions computed to measure the relative velocity change measure $d\upsilon/\upsilon$ (Doublet method).

velocity variations are insensitive to fluctuations of the noise energy at period ranges that were used to measure them. Therefore, they are likely to be related to changes of mechanical properties at depth.

3.2 Depth dependence of the seismic velocity changes

In order to estimate what parts of the crust are affected by the seismic velocity perturbation, we perform an inversion of the velocity variations obtained at different period bands to obtain the

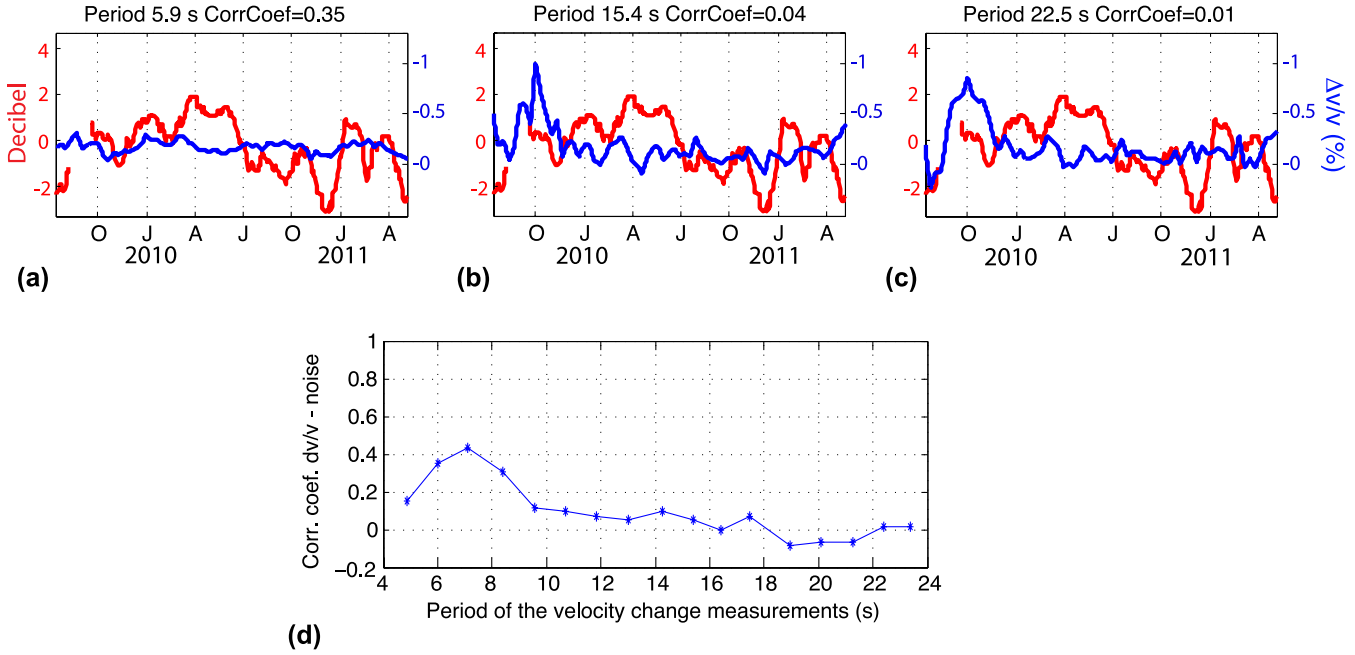

Figure 4. Comparison between the median filtered noise energy over 40-d time window measured in the 10–20 s period band (red curves) and the waves speed variation (blue curves) calculated at different period bands: 5.0–6.8, 13–17.9 and 19–26 s with central period respectively of $T = 5.9$ s (a), $T = 15.4$ s (b) and $T = 22.5$ s (c). The central period of the velocity variation and the correlation coefficient between the velocity variation and the noise energy measured in the 10–20 s period band are indicated on top of each plot. (d) Correlation coefficient computed between the noise energy between 10 and 20 s and the seismic velocity variations observed at different period bands.

velocity variation as a function of depth. Because the observed velocity changes have small amplitudes, we use a linearized approach (e.g. Aki & Richards 2002), implemented by Herrmann (2002) in his 'Computer Programs in Seismology'. The initial dispersion curve is computed with the 1-D velocity model proposed by Campillo *et al.* (1996). From this velocity model we compute the phase velocity dispersion curve of Rayleigh waves. This initial dispersion curve is then modified to take into account the relative velocity changes measured previously at different period bands. After a linearized inversion of this modified dispersion curve, we obtain the *S*-waves velocity differences between our initial model and the final model as a function of time and depth (Fig. 5a). We compute the resolution matrix of the inverse problem (Fig. S9) to estimate the robustness of our inversion.

The observations of wave speed variations are up to 23.50 s of central period. The resolution matrix shows that this gives a satisfactory resolution down to 20 km and thus we can see that the velocity perturbation does not affect the first 10 km of the crust (Fig. 5a). Fig. S10 shows the perturbation of *S*-wave velocity as a function of depth at four dates indicated as *i*, *j*, *k*, *l* in Fig. 5(a). This inversion of the velocity changes at depth shows that the shallow part of the crust is not involved in the velocity decrease that maximizes in the mid-lower crust.

3.3 Elastic modelling of the 2009–2010 SSE

The velocity perturbation at periods longer than 12 s reaches its maximum in 2009 October and then recovers to its average value after 2 months. On the other hand, the first subevent of the 2009–2010 SSE slip sequence lasted approximately 8 months and the second subevent lasted 6 months. Rapid relaxation of the velocity perturbation in comparison with the slip duration suggests that the change in wave speed in not related directly to the strain produced by the SSE.

To better understand the origin of the velocity change in term of perturbation of the mechanical properties, we computed a quasi-static time evolution of the 3-D elastic strain field associated with the 2009–2010 SSE. We used an elastic 3-D finite-difference code (Olsen *et al.* 2009) with the following model settings: the 2-D velocity structure below the Guerrero province (Iglesias *et al.* 2010), the geometry of the subduction interface determined from receiver function analysis (Pérez-Campos *et al.* 2008), and the slip model of the 2009–2010 SSE (Radiguet 2011). We focus in particular on volumetric strain or dilation because it affects both the velocities of *P* and *S* waves that form Rayleigh waves.

We perform a spatial average of the dilation beneath our seismic network for each depth. We then average over the 40-d time window to obtain the daily rate of the dilation presented in Fig. 5(c). We observe that the maximum rate of dilation occurred from 2009 September to November, at the time when the seismic velocity perturbation reached its maximum (Fig. 5a). In addition, the duration of the velocity perturbation is of the same order of the duration of the high strain rate episode. Another variation of seismic wave speed is observed at the time of the slip initiation of the second subevent (2010 March) that is also associated with an increase in the dilation rate. In this case, the dilation rate remains high and lasts longer than the velocity perturbation. However, the slip model is not accurate enough to resolve well a low amplitude slip at the beginning of the second subevent slip sequence. Nevertheless a relationship between seismic velocity changes and strain rate produced by the SSE is rather evident. Rivet *et al.* (2011) observed the same correlation for the 2006 SSE in Guerrero region using a data set from a different seismic network (the Meso American Seismic Experiment). The observed velocity variations suggest that mechanical properties of the upper plate are affected by the strain rate changes produced

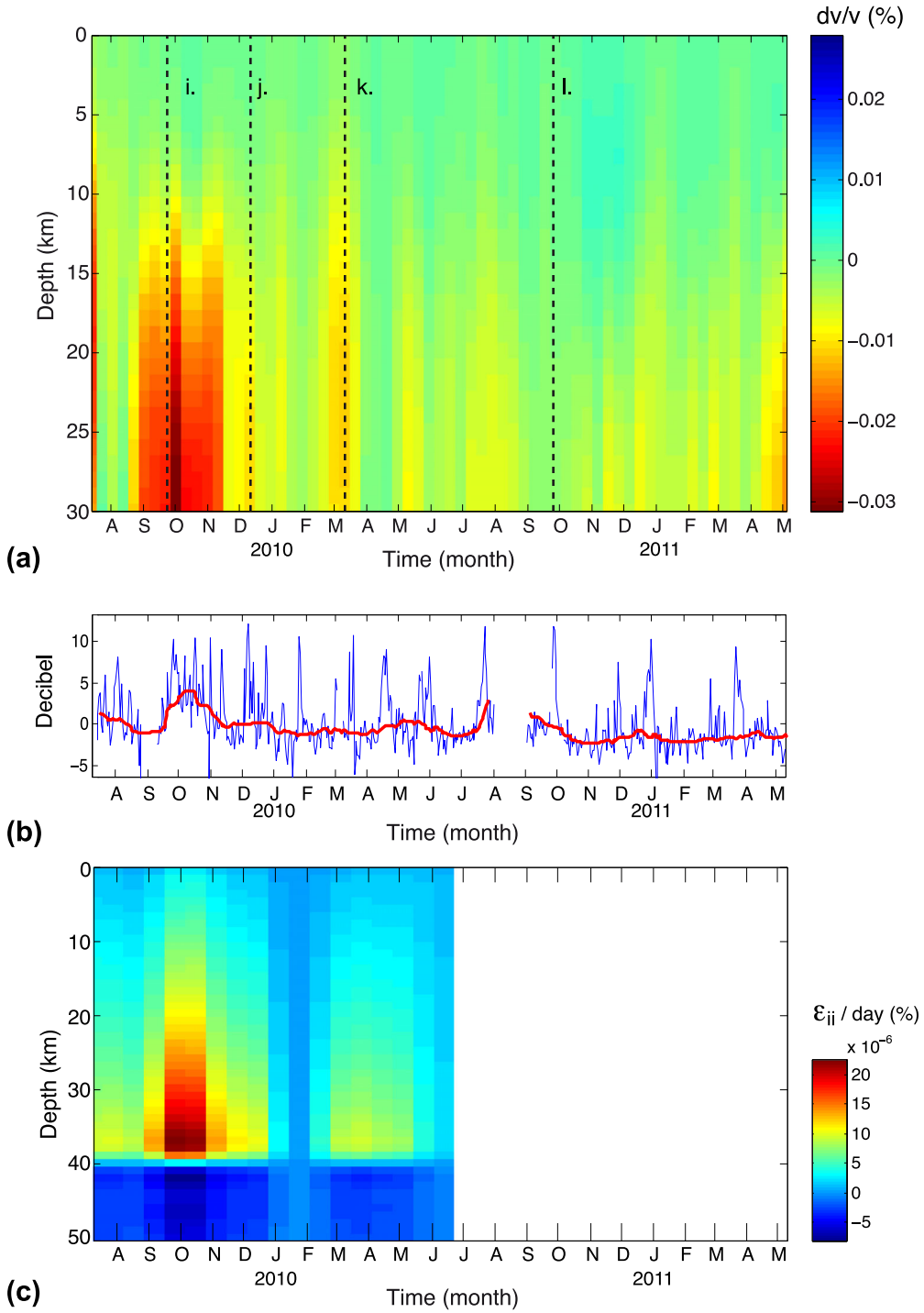

Figure 5. (a) *S*-wave relative velocity changes as a function of depth. Velocity change at time *i*, *j*, *k, l* are shown Fig. S10. (b) Non-volcanic tremor energy at ARIG station estimated at frequency range between 2 and 7 Hz. Median filters over 4 d (blue curve) and 40-d (red curve) were applied to the noise energy. (c) Evolution of dilation per day (ε_{ii} per day) averaged over a period of 20 d computed in an elastic medium from the SSE slipping model (Radiguet 2011).

during the SSE. Based on these observations, we propose to use temporal velocity anomalies at depth as a proxy of the strain rate changes in the overriding plate crust.

3.4 Relation between the seismic velocity changes and the NVTs

In Section 3.3, we argued that the velocity changes could be seen as a proxy of strain rate in the crust. If this hypothesis is true, it may imply some relations between velocity changes and other transient phenomenon such as NVTs. In this section, we further investigate the relation between the observed seismic velocity changes and the NVT activity at the seismic station ARIG (see map Fig. 1). The NVT energy is estimated from the squared velocities of the vertical component and is dominant in the frequency band between 2 and 7 Hz (Fig. 5b). Two different median filters were applied to the time-series. The first one is a short 4-d median filter that highlights short duration high energy NVT activity. The second median filter,

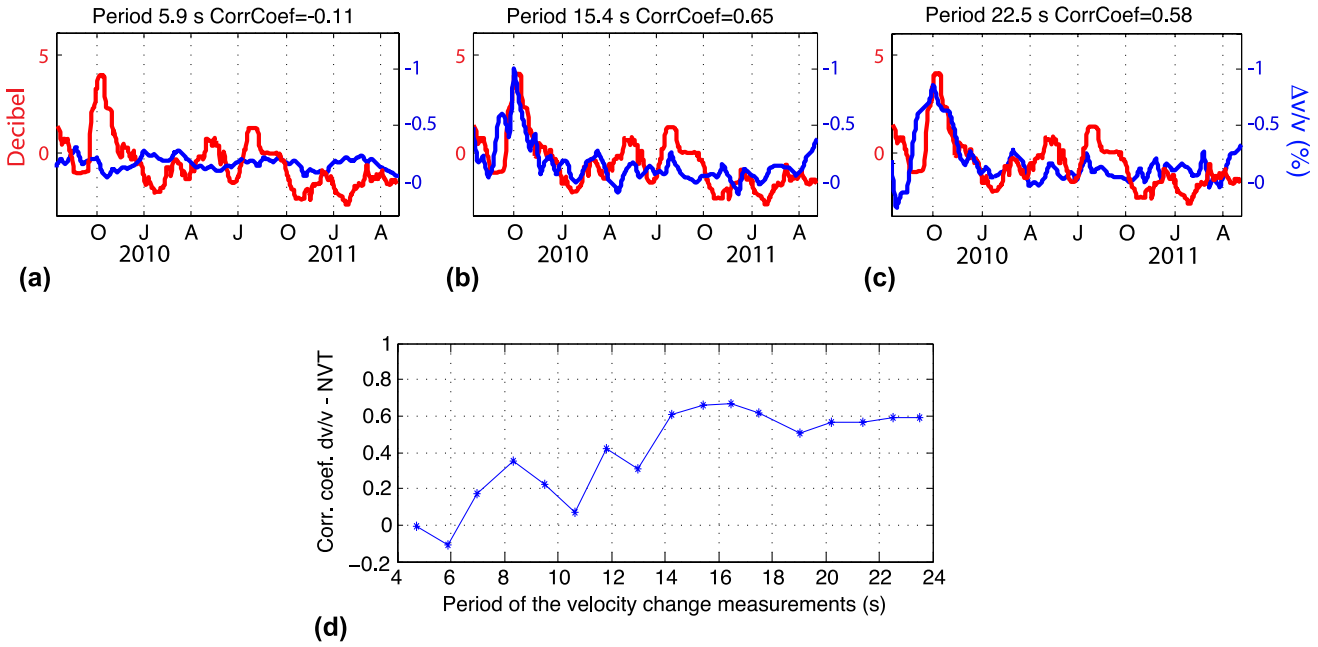

Figure 6. Comparison between the median filtered NVT energy over 40-d time window calculated between 2 and 7 Hz (red curves) and the seismic waves speed variation (blue curves) calculated at different period bands: 5.0–6.8 s, 13–17.9 s and 19–26 s with central period respectively of $T = 5.9$ s (a), $T = 15.4$ s (b) and $T = 22.5$ s (c). The central period of the velocity variation and the correlation coefficient between the velocity variation and the NVT energy are indicated on top of each plot. (d) Correlation coefficient computed between the NVT energy and the seismic velocity change observed at different period bands.

calculated on 40-d time windows, is used in order to compare NVT activity with both variations in seismic velocity perturbation and volumetric strain estimated in the same period of time. This long time window avoids the influence of short and very strong events (e.g. Husker *et al.* 2010; Kostoglodov *et al.* 2010; Zigone *et al.* 2012). From 2010 mid-September to December, the level of activity is high compared to the baseline level of the background activity (about 50 dB). This period of high activity coincides with both the drop in seismic velocity produced by the first subevent (Fig. 5a), and the maximum strain rate (Fig. 5c). This suggests that the tremor activity, along with a decrease in seismic wave velocity, is related to the slip rate at the interface during the SSE. However, several periods of strong tremor activity are observed at other times for which slip is not clearly detected. These activities have characteristic durations of the order of 10 d, shorter than the duration of the NVT high activity during the velocity change observed from mid-September to December. It can be noted that moderate SSE ($M_w < 6$) can hardly be distinguished in GPS time-series.

To evaluate carefully the relation between velocity changes and NVT activity we compare the evolution of the seismic velocity changes with the median NVT energy, both estimated on 40-d time windows of continuous seismic signals. We first measured the tremor activity between 2009 and 2011 from the average of the energy measured at three stations, ARIG, ATLI and APAX located in the northern part of Guerrero state, where NVTs are usually detected (Payero *et al.* 2008; Husker *et al.* 2012; Zigone *et al.* 2012; see the Supporting Information for details). Figs 6(a)–(c) show the evolution of both the energy of the tremor and the seismic wave speed variations calculated for three different period ranges with central periods, respectively of 5.9, 15.4 and 22.5 s. Notice that the similarity between the seismic velocity change and the NVT energy variations degrades at short periods. This is illustrated in Fig. 6(d) that shows the evolution of the correlation coefficients between changes in seismic velocity at different period bands (Table 3) and energy of tremors. This measure helps to quantify the relationship between these two observables. For periods less than 12 s, the velocity variations are weakly correlated with the energy of tremors; the correlation coefficient is less than 0.4. Beyond 14 s of central period, the correlation between the two measures increases and reaches 0.7 at around 16 s. Then the correlation stabilizes at 0.6 at longer periods. This comparison confirms a close relation between the seismic velocity change and the NVT activity, in the period range for which we have identified variations in velocity produced by the SSE (i.e. between 14 and 24 s).

4 DISCUSSIONS

4.1 Velocity changes associated with a complex SSE

The analysis of the velocity variations associated with the SSE of 2009–2010 shows that slow deformations affect the seismic velocities in the crust. Indeed, the maximum rate of mid-lower crustal dilation coincides with a distinctive reduction of the seismic wave velocity. A similar observation was previously reported for the 2006 SSE (Rivet *et al.* 2011), however in the case of the 2009–2010 SSE, the slip sequence was more complex. Theses new observations of velocity changes confirm the link between waves speed variations and rate of deformation.

Walpersdorf *et al.* (2011) and Radiguet (2011) showed that the first subevent of the 2009–2011 SSE slip sequence occurred west of the seismological network with an amplitude 1.5 times larger than the second subevent that initiated east of the network 10 months later (Fig. S5). Due to the location of the seismic network relative to the slipping zones, we expected that the network would be more sensitive to perturbation related to the first rather than the second subevent. Indeed, it appears that the change in wave speed measured during the first subevent is larger than during the later that produced a slight decrease in the seismic velocity at its initiation in 2010 March. At this time, the velocity perturbation is about three times

lower than during the first subevent. Similarly, the rate of dilation observed for the second subevent is also about three times lower than the first subevent. This similarity between speed variation and strain rate suggests that the velocity variations could be used as a first-order indicator of the dilation rate within the crust.

4.2 Insights into the non-linear behaviour of the crust

The short durations of the velocity perturbation (∼2 months) in comparison to the elastic strain increase suggests that the velocity is not linearly related to the strain in the medium. Besides the magnitude of the velocity perturbation is of the order of 10^{-3}, while the strain involved are of the order of 10^{-6}. In linear elasticity, the velocity changes should be of the same order as the dilation (see Supporting Information). We propose to interpret observations of seismic velocity changes in the framework of non-linear elasticity. The dynamics of the rearrangement of cracks, pores and bonds between hard grains may explain the decrease of elastic modulus observed in laboratory experiments on rock samples under dynamic loading (Ostrovsky & Johnson 2001). The non-linear effects are usually observed for a deformation greater than 10^{-6} and typically produce a rapid decrease of the velocity followed by a slower and gradual return to the baseline level (TenCate & Shankland 1996; Johnson & Jia 2005; Johnson & Sutin 2005). These non-linear effects may be strongly enhanced by an increase in the pore pressure (Johnson & Jia 2005). In Guerrero, the typical volumetric strain produced by SSE is of the order of 10^{-6}, which is the threshold for non-linear elastic behaviour in laboratory experiments. Besides, fluids released in the crust due to metamorphic dehydration and high pore pressure (Jodicke *et al.* 2006; Song *et al.* 2009) could increase the pore pressure and contribute to the non-linear behaviour of the crust. During SSEs, small stress drop of 0.1–0.2 MPa (Radiguet *et al.* 2012), which are 10–100 times less than for regular earthquakes, suggest high pore pressure and low effective normal stress at the subduction interface. As proposed by SSE frictional models, an increase in dilation occurring simultaneously with the SSE tends to reduce this high pore pressure at the interface, and thus acts as a strengthening force, favouring steady slip (e.g. Segall *et al.* 2010) and preventing the plate interface to become dynamically instable. Finally poroelasticity may also contribute to the decrease of the observed seismic velocity and its recovery since it affects large-scale fluid motions within the crust.

4.3 A complex relation between NVT and SSE

In most subduction zones where SSEs have been detected, they are associated with NVT episodes. The tremor often occurs in the close vicinity of the SSE, like in Cascades (Gomberg *et al.* 2010), Nankai (Japan) (Hirose & Obara 2010) and Alaska (Peterson & Christensen 2009). Bartlow *et al.* (2011) showed recently that during the 2009 SSE in Cascadia, the tremors concentrated in areas where the slow slip rate was maximal, following the slip front. The authors interpret these tremors as frictional heterogeneities that reach a slip velocity adequate for the emission of seismic waves. In Guerrero, a comparison between NVT epicenters and the area of slow slip at the subduction interface during the 2006 SSE shows that a relatively small cluster of tremors is triggered by the sliding front of the SSE, and are probably related to the shear stress accumulation (Husker *et al.* 2012). This particular NVT cluster represents only a small fraction of the entire tremor activity. In terms of seismic energy, these NVT are two to three times less energetic than those occurring farther north, outside of the 2006 SSE area (Payero *et al.* 2008; Kostoglodov *et al.* 2010; Husker *et al.* 2012). It is thus difficult to explain most of NVT in the Guerrero subduction zone by mechanical models that describe tremors as a result of frictional instabilities at the interface of the slipping zone during SSE (Obara & Hirose 2006; Shelly *et al*. 2006, 2007; Ide *et al.* 2007; Kao *et al.* 2007; Brown *et al.* 2009; Ghosh *et al.* 2009; La Rocca *et al.* 2009; Larmat *et al.* 2009). Seismological and geodetic observations in Guerrero do not support this model and different explanations are needed to explain the spatial and energetic non-conformity of NVT associated to SSEs.

4.4 Relation between NVTs, SSE and seismic velocity changes

In Guerrero, the observations of a reduction of the seismic velocity extending at depth in the crust during the SSEs in 2006 and 2009–2010 indicate that the crust undergoes volumetric strain rate high enough to induce non-linear elastic response. The analysis of the 2009–2010 SSE shows that there is a significant correlation between the NVT activity and the variations of the seismic wave speeds suggesting that these two different and independent observations can be linked to a single mechanism. The correlation between velocity change and NVT energy suggests that the increase in dilatation caused by the SSE can produce simultaneously the drop of velocity within the crust and enhanced NVTs activity, either at the subduction interface or on secondary faults and cracks in the crust. This activity could be linked to changes of effective pressure during the SSE as suggested by recent mechanical models involving dilatancy (Segall *et al.* 2010). Furthermore, high rate dilation can affect areas away from the slipping plate interface and therefore might enhance NVT activity distant from the main fault (SSE slipping zone).

For the periods without large SSEs, Vergnolle *et al.* (2010) and Zigone *et al.* (2012) highlighted the coincidence of high strain rate periods, as revealed by careful analysis of GPS time-series, with the occurrence of NVTs. Zigone *et al.* (2012) showed that the increase of NVT activity in Guerrero was associated with some peaks of displacement velocity of the American Plate in the southern direction, indicative of slow slip episodes.

The correlation between temporal variations in seismic speed and tremor activity (Fig. 6), and their apparent relation with the 2009–2010 SSE suggests that the crustal velocity changes as well as high NVT episodes are related to the increases of strain rate associated with SSEs and can be considered as markers of the SSEs barely detected with GPS. However, the hypothesis that high frequency NVT themselves could produce a velocity decrease in the lower crust cannot be discarded. Recent laboratory experiments (Johnson *et al.* 2012) suggest that insonation at high frequency of a rock sample produces a reduction of the elastic parameters. Further quantitative studies are needed to evaluate the expected threshold of amplitude for the non-elastic behaviour and to evaluate how far the shaking from tremor could be responsible for a velocity reduction.

5 CONCLUSION

The results obtained in this study are in good agreement with those obtained previously for the 2006 Guerrero SSE and confirm that the crust presents a non-linear behaviour when subject to relatively low strain. Through the study of waves speed variations produced by the 2009–2010 SSE, we show that the relative velocity change is a robust measure that is correlated with the dilation rate at depth.

With the new data acquired during the 2009–2010 SSE, we study simultaneously changes in wave velocity and the energy of NVTs. A good correlation between NVTs activity and velocity changes during 2009–2011 suggests a relation between the deformation of the overriding plate and the NVTs. A joint analysis of these various observations highlights the importance of the strain increase within the crust, which is associated with velocity decrease and NVT occurrence. These observations suggest that both NVTs and seismic speed variation can be used as a proxy of the strain rate at depth.

ACKNOWLEDGEMENTS

This study was supported by the Agence National de la Recherche (France) under the contract RA0000CO69 'G-GAP', by the European Research Council Advanced Grant 227507 «Whisper» and by project grants form CONACYT 84544 and PAPIIT IN110611 and IN103808. We are grateful to all people who participated in the seismic antennas installation and maintenance. We thank Paul Johnson and other G-GAP participants (Allen Husker, Guillaume Bacques) for their stimulating discussions. We thank Catherine Pequegnat and Ekaterina Bourova-Flin for their work on the management of the seismological database.

REFERENCES

Aki, K. & Richards, P., 2002. *Quantitative Seismology,* University Science Books.

Altamimi, Z., Collilieux, X. & Métivier, L., 2011. Itrf2008: an improved solution of the international terrestrial reference frame, *J. Geod.,* **85**(8), 457–473.

Bartlow, N., Miyazaki, S., Bradley, A. & Segall, P., 2011. Space-time correlation of slip and tremor during the 2009 Cascadia slow slip event, *Geophys. Res. Lett.,* **38**(18), L18309, doi:10.1029/2011GL048714.

Brenguier, F., Campillo, M., Hadziioannou, C., Shapiro, N.M., Nadeau, R.M. & Larose, E., 2008a. Postseismic relaxation along the San Andreas fault at Parkfield from continuous seismological observations, *Science,* **321**(5895), 1478–1481.

Brenguier, F., Shapiro, N.M., Campillo, M., Ferrazzini, V., Duputel, Z., Coutant, O. & Nercessian, A., 2008b. Towards forecasting volcanic eruptions using seismic noise, *Nat. Geosci.,* **1**(2), 126–130.

Brown, J.R. *et al.*, 2009. Deep low-frequency earthquakes in tremor localize to the plate interface in multiple subduction zones, *Geophys. Res. Lett.,* **36,** L19306, doi:10.1029/2009GL040027.

Brown, K.M., Tryon, M.D., DeShon, H.R., Dorman, L.M. & Schwartz, S.Y., 2005. Correlated transient fluid pulsing and seismic tremor in the Costa Rica subduction zone, *Earth planet. Sci. Lett.,* **238**(1–2), 189–203.

Campillo, M. & Paul, A., 2003. Long-range correlations in the diffuse seismic coda, *Science,* **299**(5606), 547–549.

Campillo, M., Singh, S., Shapiro, N., Pacheco, J. & Herrmann, R., 1996. Crustal structure south of the Mexican volcanic belt, based on group velocity dispersion, *Geof. Int. - Mexico,* **35,** 361–370.

Chen, J.H., Froment, B., Liu, Q.Y. & Campillo, M., 2010. Distribution of seismic wave speed changes associated with the 12 May 2008 M_W 7.9 Wenchuan earthquake, *Geophys. Res. Lett.,* **37,** L18302, doi:10.1029/2010GL044582.

Clarke, D., Zaccarelli, L., Shapiro, N.M. & Brenguier, F., 2011. Assessment of resolution and accuracy of the Moving Window Cross Spectral technique for monitoring crustal temporal variations using ambient seismic noise, *Geophys. J. Int.,* **186,** 867–882.

Delahaye, E.J., Townend, J., Reyners, M.E. & Rogers, G., 2009. Microseismicity but no tremor accompanying slow slip in the Hikurangi subduction zone, New Zealand, *Earth planet. Sci. Lett.,* **277**(1–2), 21–28.

DeMets, C., Gordon, R.G., Argus, D.F. & Stein, S., 1994. Effect of recent revisions to the geomagnetic reversal time-scale on estimates of current plate motions, *Geophys. Res. Lett.,* **21**(20), 2191–2194.

Froment, B., Campillo, M., Roux, P., Gouedard, P., Verdel, A. & Weaver, R.L., 2010. Estimation of the effect of nonisotropically distributed energy on the apparent arrival time in correlations, *Geophysics,* **75**(5), SA85–SA93.

Ghosh, A., Vidale, J.E., Sweet, J.R., Creager, K.C. & Wech, A.G., 2009. Tremor patches in Cascadia revealed by seismic array analysis, *Geophys. Res. Lett.,* **36,** L17316, doi:10.1029/2009GL039080.

Gomberg, J. *et al.*, 2010. Slow-slip phenomena in Cascadia from 2007 and beyond: a review, *Bull. geol. Soc. Am.,* **122**(7–8), 963–978.

Hadziioannou, C., Larose, E., Coutant, O., Roux, P. & Campillo, M., 2009. Stability of monitoring weak changes in multiply scattering media with ambient noise correlation: laboratory experiments, *J. acoust. Soc. Am.,* **125**(6), 3688–3695.

Hennino, R., Tregoures, N., Shapiro, N., Margerin, L., Campillo, M., van Tiggelen, B. & Weaver, R., 2001. Observation of equipartition of seismic waves, *Phys. Rev. Lett.,* **86**(15), 3447–3450.

Herrmann, R., 2002. *Computer Programs in Seismology*, Version 3.15, Saint Louis University.

Hillers, G., Graham, N., Campillo, M., Kedar, S., Landès, M. & Shapiro, N., 2012. Global oceanic microseism sources as seen by seismic arrays and predicted by wave action models, *Geochem. Geophys. Geosyst.,* **13,** Q01021, doi:10.1029/2011GC003875.

Hirose, H. & Obara, K., 2010. Recurrence behavior of short-term slow slip and correlated Nonvolcanic tremor episodes in western Shikoku, southwest Japan, *J. geophys. Res.,* **115,** B00A21, doi:10.1029/2008JB006050.

Hirose, H., Asano, Y., Obara, K., Kimura, T., Matsuzawa, T., Tanaka, S. & Maeda, T., 2010. Slow earthquakes linked along dip in the Nankai subduction zone, *Science,* **330**(6010), 1502, doi: 10.1126/science.

Husker, A., Peyrat, S., Shapiro, N. & Kostoglodov, V., 2010. Automatic non-volcanic tremor detection in the Mexican subduction zone, *Geof. Int. - Mexico,* **49**(1), 17–25.

Husker, A., Kostoglodov, V., Cruz-Atienza, V., Legrand, D., Shapiro, N., Payero, J., Campillo, M. & Huesca-Pérez, E., 2012. Temporal variations of non-volcanic tremor (NVT) locations in the Mexican subduction zone: finding the NVT sweet spot, *Geochem. Geophys. Geosyst.,* **13,** Q03011, doi:10.1029/2011GC003916.

Ide, S., Shelly, D.R. & Beroza, G.C., 2007. Mechanism of deep low frequency earthquakes: further evidence that deep non-volcanic tremor is generated by shear slip on the plate interface, *Geophys. Res. Lett.,* **34,** L03308, doi:10.1029/2006GL028890.

Iglesias, A., Clayton, R.W., Perez-Campos, X., Singh, S.K., Pacheco, J.F., Garcia, D. & Valdes-Gonzalez, C., 2010. S wave velocity structure below central Mexico using high-resolution surface wave tomography, *J. geophys. Res.-Solid Earth,* **115**(B6), B06307, doi:10.1029/2009JB006332.

Jodicke, H., Jording, A., Ferrari, L., Arzate, J., Mezger, K. & Rupke, L., 2006. Fluid release from the subducted Cocos plate and partial melting of the crust deduced from magnetotelluric studies in southern Mexico: implications for the generation of volcanism and subduction dynamics, *J. geophys. Res.-Solid Earth,* **111,** B08102, doi:10.1029/2005JB003739.

Johnson, P. & Sutin, A., 2005. Slow dynamics and anomalous nonlinear fast dynamics in diverse solids, *J. acoust. Soc. Am.,* **117**(1), 124–130.

Johnson, P.A. & Jia, X., 2005. Nonlinear dynamics, granular media and dynamic earthquake triggering, *Nature,* **437**(7060), 871–874.

Johnson, P.A., Carpenter, B., Knuth, M., Kaproth, B.M., Le Bas, P.-Y., Daub, E.G. & Marone, C., 2012. Nonlinear dynamical triggering of slow slip on simulated earthquake faults with implications to Earth, *J. geophys. Res.,* **117**(B04), B04310, doi:10.1029/2011JB008594.

Kao, H., Shan, S.J., Dragert, H., Rogers, G., Cassidy, J.F. & Ramachandran, K., 2005. A wide depth distribution of seismic tremors along the northern Cascadia margin, *Nature,* **436**(7052), 841–844.

Kao, H., Shan, S.J., Rogers, G. & Dragert, H., 2007. Migration characteristics of seismic tremors in the northern Cascadia margin, *Geophys. Res. Lett.,* **34,** L03304, doi:10.1029/2006GL028430.

Kim, M.J., Schwartz, S.Y. & Bannister, S., 2011. Non-volcanic tremor associated with the March 2010 Gisborne slow slip event at the Hikurangi subduction margin, New Zealand, *Geophys. Res. Lett.,* **38**(14), L14301, doi:10.1029/2011GL048400.

Koper, K., de Foy, B. & Benz, H., 2009. Composition and variation of noise recorded at the Yellowknife seismic array, 1991–2007, *J. geophys. Res.,* **114**(B10), B10310.

Kositsky, A. & Avouac, J., 2010. Inverting geodetic time series with a principal component analysis-based inversion method, *J. geophys. Res.,* **115**(B3), B03401, doi:10.1029/2009JB006535.

Kostoglodov, V., Husker, A., Shapiro, N.M., Payero, J.S., Campillo, M., Cotte, N. & Clayton, R., 2010. The 2006 slow slip event and nonvolcanic tremor in the Mexican subduction zone, *Geophys. Res. Lett.,* **37,** L24301, doi:10.1029/2010GL045424.

La Rocca, M., Creager, K., Galluzzo, D., Malone, S., Vidale, J., Sweet, J. & Wech, A., 2009. Cascadia tremor located near plate interface constrained by S minus P wave times, *Science,* **323**(323), 620–623.

Landès, M., Hubans, F., Shapiro, N., Paul, A. & Campillo, M., 2010. Origin of deep ocean microseisms by using teleseismic body waves, *J. geophys. Res.,* **115,** B05302, doi:10.1029/2009JB006918.

Larmat, C.S., Guyer, R.A. & Johnson, P.A., 2009. Tremor source location using time reversal: selecting the appropriate imaging field, *Geophys. Res. Lett.,* **36,** doi:10.1029/2009GL040099.

Larson, K.M., Kostoglodov, V., Miyazaki, S. & Santiago, J.A.S., 2007. The 2006 aseismic slow slip event in Guerrero, Mexico: new results from GPS, *Geophys. Res. Lett.,* **34,** L13309, doi:10.1029/2007GL029912.

Lobkis, O. & Weaver, R., 2003. Coda-wave interferometry in finite solids: recovery of p-to-s conversion rates in an elastodynamic billiard, *Phys. Rev. Lett.,* **90**(25), 254–302.

McCaffrey, R., Wallace, L. & Beavan, J., 2008. Slow slip and frictional transition at low temperature at the Hikurangi subduction zone, *Nat. Geosci.,* **1**(5), 316–320.

Margerin, L., Campillo, M., Van Tiggelen, B.A. & Hennino, R., 2009. Energy partition of seismic coda waves in layered media: theory and application to Pinyon Flats Observatory, *Geophys. J. Int.,* **177**(2), 571–585.

Nugraha, A. & Mori, J., 2006. Three-dimensional velocity structure in the Bungo channel and Shikoku area, Japan, and its relationship to low-frequency earthquakes, *Geophys. Res. Lett.,* **33**(24), L24307, doi:10.1029/2006GL028479.

Obara, K., 2002. Nonvolcanic deep tremor associated with subduction in southwest Japan, *Science,* **296**(5573), 1679–1681.

Obara, K., 2011. Characteristics and interactions between non-volcanic tremor and related slow earthquakes in the Nankai subduction zone, southwest Japan, *J. Geodyn.,* **52,** 229–248.

Obara, K. & Hirose, H., 2006. Non-volcanic deep low-frequency tremors accompanying slow slips in the southwest Japan subduction zone, *Tectonophysics,* **417**(1–2), 33–51.

Obara, K., Hirose, H., Yamamizu, F. & Kasahara, K., 2004. Episodic slow slip events accompanied by non-volcanic tremors in southwest Japan subduction zone, *Geophys. Res. Lett.,* **31,** L23602, doi:10.1029/2004GL020848.

Obermann, A., Planes, T., Larose, E., Sens-Schonfelder, C. & Campillo, M., 2013. Depth sensitivity of seismic coda waves to velocity perturbations in an elastic heterogeneous medium, *Geophys. J. Int.,* **194**(1), 372–382.

Ohta, K. & Ide, S., 2008. A precise hypocenter determination method using network correlation coefficients and its application to deep low-frequency earthquakes, *Earth Planets Space,* **60**(8), 877–882.

Ohta, Y., Freymueller, J., Hreinsdottir, S. & Suito, H., 2006. A large slow slip event and the depth of the seismogenic zone in the south central Alaska subduction zone, *Earth planet. Sci. Lett.,* **247**(1–2), 108–116.

Olsen, K.B. *et al.*, 2009. ShakeOut-D: ground motion estimates using an ensemble of large earthquakes on the southern San Andreas fault with spontaneous rupture propagation, *Geophys. Res. Lett.,* **36,** L04303, doi:10.1029/2008GL036832.

Ostrovsky, L.A. & Johnson, P., 2001. Dynamic non-linear elasticity in geomaterial, *Rivista del nuovo cimento,* **24**(7), 1–46.

Ozawa, S., Suito, H. & Tobita, M., 2007. Occurrence of quasi-periodic slow-slip off the east coast of the Boso peninsula, central Japan, *Earth Planets Space,* **59**(12), 1241–1245.

Payero, J.S., Kostoglodov, V., Shapiro, N., Mikumo, T., Iglesias, A., Perez-Campos, X. & Clayton, R.W., 2008. Nonvolcanic tremor observed in the Mexican subduction zone, *Geophys. Res. Lett.,* **35,** L07305, doi:10.1029/2007GL032877.

Pérez-Campos, X. *et al.*, 2008. Horizontal subduction and truncation of the Cocos plate beneath central Mexico, *Geophys. Res. Lett.,* **35**(18), L18303, doi:10.1029/2008GL035127.

Peterson, C.L. & Christensen, D.H., 2009. Possible relationship between nonvolcanic tremor and the 1998–2001 slow slip event, south central Alaska, *J. geophys. Res.-Solid Earth,* **114,** B06302, doi:10.1029/2008JB006096.

Poupinet, G., Ellsworth, W.L. & Frechet, J., 1984. Monitoring velocity variations in the crust using earthquake doublets - An application to the Calaveras fault, California, *J. geophys. Res.,* **89**(NB7), 5719–5731.

Radiguet, M., 2011. Etude des séismes lents et du chargement intersismique dans la lacune sismique de Guerrero au Mexique, *PhD thesis*, Université Joseph Fourier, ISTERRE.

Radiguet, M., Cotton, F., Vergnolle, M., Campillo, M., Valette, B., Kostoglodov, V. & Cotte, N., 2011. Spatial and temporal evolution of a long term slow slip event, the 2006 Guerrero slow slip event, *Geophys. J. Int.,* **184**(2), 816–828.

Radiguet, M., Cotton, F., Vergnolle, M., Campillo, M., Walpersdorf, A., Cotte, N. & Kostoglodov, V., 2012. Slow slip events and strain accumulation in the Guerrero gap, Mexico, *J. geophys. Res.,* **117**(B4), B04305, doi:10.1029/2011JB008801.

Rivet, D., Campillo, M., Shapiro, N.M., Cruz-Atienza, V., Radiguet, M., Cotte, N. & Kostoglodov, V., 2011. Seismic evidence of nonlinear crustal deformation during a large slow slip event in Mexico, *Geophys. Res. Lett.,* **38,** L08308, doi:10.1029/2011GL047151.

Rogers, G. & Dragert, H., 2003. Episodic tremor and slip on the Cascadia subduction zone: the chatter of silent slip, *Science,* **300**(5627), 1942–1943.

Rubinstein, J., Shelly, D. & Ellsworth, W., 2010. Non-volcanic tremor: a window into the roots of fault zones, in *New Frontiers in Integrated Solid Earth Sciences,* pp. 287–314, eds Cloetingh, S. & Negendank, J., Springer.

Schimmel, M., Stutzmann, E., Ardhuin, F. & Gallart, J., 2011. Polarized earth's ambient microseismic noise, *Geochem. Geophys. Geosyst.,* **12**(7), Q07014, doi:10.1029/2011GC003661.

Schwartz, S. & Rokosky, J., 2007. Slow slip events and seismic tremor at circum-Pacific subduction zones, *Rev. Geophys.,* **45,** RG3004, doi:10.1029/2006RG000208.

Segall, P., Rubin, A., Bradley, A. & Rice, J., 2010. Dilatant strengthening as a mechanism for slow slip events, *J. geophys. Res.,* **115,** B12305, doi:10.1029/2010JB007449.

Shapiro, N. & Campillo, M., 2004. Emergence of broadband Rayleigh waves from correlations of the ambient seismic noise, *Geophys. Res. Lett.,* **31,** L07614, doi:10.1029/2004GL019491.

Shelly, D.R., Beroza, G.C., Ide, S. & Nakamula, S., 2006. Low-frequency earthquakes in Shikoku, Japan, and their relationship to episodic tremor and slip, *Nature,* **442**(7099), 188–191.

Shelly, D.R., Beroza, G.C. & Ide, S., 2007. Non-volcanic tremor and low-frequency earthquake swarms, *Nature,* **446**(7133), 305–307.

Song, T.R.A., Helmberger, D.V., Brudzinski, M.R., Clayton, R.W., Davis, P., Perez-Campos, X. & Singh, S.K., 2009. Subducting slab ultra-slow velocity layer coincident with silent earthquakes in Southern Mexico, *Science,* **324**(5926), 502–506.

Stehly, L., Campillo, M. & Shapiro, N.M., 2006. A study of the seismic noise from its long-range correlation properties, *J. geophys. Res.-Solid Earth,* **111,** B10306, doi:10.1029/2005JB004237.

Stutzmann, E., Schimmel, M., Patau, G. & Maggi, A., 2009. Global climate imprint on seismic noise, *Geochem. Geophys. Geosyst.,* **10,** Q11004, doi:10.1029/ 2009GC002619.

Tanimoto, T., Ishimaru, S. & Alvizuri, C., 2006. Seasonality of particle motion of microseisms, *Geophys. J. Int.,* **166,** 253–266.

TenCate, J.A. & Shankland, T.J., 1996. Slow dynamics in the nonlinear elastic response of Berea sandstone, *Geophys. Res. Lett.,* **23**(21), 3019–3022.

Vergnolle, M., Walpersdorf, A., Kostoglodov, V., Tregoning, P., Santiago, J.A., Cotte, N. & Franco, S.I., 2010. Slow slip events in Mexico

revised from the processing of 11 year GPS observations, *J. Geophys. Res.,* **115**(B8), B08403, doi:10.1029/2009JB006852.
Walpersdorf, A., Cotte, N., Kostoglodov, V., Vergnolle, M., Radiguet, M., Antonio Santiago, J. & Campillo, M., 2011. Two successive slow slip events evidenced in 2009–2010 by a dense GPS network in Guerrero, Mexico, *Geophys. Res. Lett.,* **38,** L15307, doi:10.1029/2011GL048124.
Weaver, R., Froment, B. & Campillo, M., 2009. On the correlation of non-isotropically distributed ballistic scalar diffuse waves, *J. acoust. Soc. Am.,* **126**(4), 1817–1826.
Weaver, R.L., Hadziioannou, C., Larose, E. & Campillo, M., 2011. On the precision of noise correlation interferometry, *Geophys. J. Int.,* **185**(3), 1384–1392.
Wegler, U. & Sens-Schonfelder, C., 2007. Fault zone monitoring with passive image interferometry, *Geophys. J. Int.,* **168**(3), 1029–1033.
Zigone, D. *et al.*, 2012. Triggering of tremors and slow slip event in Guerrero, Mexico, by the 2010 M_w 8.8 Maule, Chile, earthquake, *J. geophys. Res.,* **117,** B09304, doi:10.1029/2012JB009160.

SUPPORTING INFORMATION

Additional Supporting Information may be found in the online version of this article:

Figure S1. Mini array XALI deployed during the G-GAP campaign. Six short period sensors (red triangles) surround a single broad-band sensor (yellow triangle).
Figure S2. Forty-day stacked cross-correlation functions for broad-band receiver pair APAXB-XALIB (a) and short period sensors APAX2-XALI3 (b). The cross-correlation functions are filtered between 8 and 30 s and normalized in amplitude.
Figure S3. Normalized amplitude of the noise energy flux as a function of azimuth and time, for period ranges between 4 and 9 s (a) and between 9 and 16 s (b). Periods of missing data are shown in black. The dominant noise in terms of energy comes from the Pacific Ocean (between 140° and 300° azimuth).
Figure S4. Selection of daily correlations with signal-to-noise ratio greater than 1.5. (a) Set of all the daily correlations for AMAC3-APAX4 stations before selection. (c) The same set as (a) but after selection of correlation with signal-to-noise ration greater than 1.5.
Figure S5. Comparison of the seismic velocity change for [8–20]s period band measured using, on the one hand, the method of doublets (blue curve) and on the other hand, the Stretching method (red curve). Consistency is shown for the Doublet method only. The red and green dashed lines represent respectively, the initiation of the first and second subevent of the SSE.
Figure S6. Seismic velocity change at (15–20 s) period band measured from the vertical components of noise cross-correlations computed from (a) seven broad-band sensors and (b) 51 short period sensors. (c) Time-series of daily north–south displacements recorded at CPDP (red) and CAYA (green) GPS stations with respect to ITRF2008 (Altamimi *et al.* 2011). The red and green dashed lines represent respectively, the initiation of the first and second subevent of the SSE.
Figure S7. Cumulated slip over the period of 50 sequential days during the 2009–2010 SSE obtained from the slow slip model computed by inversion of GPS time-series Radiguet (2011). The colourbar is saturated to 0.03 m, the maximum cumulated slip between 2009 September 10 and October 30 reaches 0.07. Small black arrows indicate the slip direction between *S* and SSW. The time periods are annotated on the top of each plot. Red triangles represent the G-GAP mini-arrays seismic stations used in this study. The red bracket indicates the slip period during which the slip velocity reached his maximum.
Figure S8. Sensitivity of the Rayleigh waves at 14 s period computed in the velocity model of the structure below Guerrero taken from Iglesias *et al.* (2010).
Figure S9. The resolution matrix of the inverse problem shows how the velocity variations at different depth are retrieved by the inversion. A value of one on the diagonal of the matrix would represent a perfect recovery. Here, we see the spreading over different depth. Deeper velocity variations are not well retrieved.
Figure S10. Inversion at depth of the *S*-wave relative velocity changes for four different times indicated by the lines *i*, *j*, *k*, *l*, in Fig. 5(a).
Figure S11. Evolution of the dilation rate modelled at 30 km depth (a). Median over 4 d (b) and 40 d (c) of the seismic noise energy between 2 and 7 Hz corresponding to the frequency range at which we detect non-volcanic tremors for ARIG (blue), APAX (black) and ATLI (red) seismic stations (see Fig. 1 for the station location reference).
Accounting for seasonal variations of noise sources
Average NVT energy
Relation between velocity changes and a volumetric deformation of the medium in linear elasticity (http://gji.oxfordjournals.org/lookup/suppl/doi:10.1093/gji/ggt374/-/DC1).

Please note: Oxford University Press is not responsible for the content or functionality of any supporting materials supplied by the authors. Any queries (other than missing material) should be directed to the corresponding author for the article.